

Accepted for publication in Phys. Rev. B

Dimensional crossover in a mesoscopic superconducting loop of finite width

V. Bruyndoncx*, L. Van Look, M. Verschueren, and V. V. Moshchalkov

*Laboratorium voor Vaste-Stoffysica en Magnetisme,**Katholieke Universiteit Leuven, Celestijnenlaan 200 D, B-3001 Leuven, Belgium*

(September 15, 2021)

Abstract

Superconducting structures with the size of the order of the superconducting coherence length $\xi(T)$ have a critical temperature T_c , oscillating as a function of the applied perpendicular magnetic field H (or flux Φ). For a thin-wire superconducting loop, the oscillations in T_c are perfectly periodic with H (this is the well-known Little-Parks effect), while for a singly connected superconducting disk the oscillations are pseudoperiodic, i.e. the magnetic period decreases as H grows. In the present paper, we study the intermediate case: a loop made of thick wires. By increasing the size of the opening in the middle, the disk-like behaviour of $T_c(H)$ with a quasi-linear background (characteristic for '3-dimensional' (3D) behaviour) is shown to evolve into a parabolic $T_c(H)$ background ('2D'), superimposed with perfectly periodic oscillations. The calculations are performed using the linearized Ginzburg-Landau theory, with the proper normal/vacuum boundary conditions at both the internal and the external interface. Above a certain crossover magnetic flux Φ , $T_c(\Phi)$ of the loops becomes quasi-linear, and the flux period matches with the case of the filled disk. This dimensional transition is similar to the 2D-3D transition for thin films in a parallel magnetic field, where vortices enter the material as soon as the film thickness $t > 1.8\xi(T)$. For the loops studied here, the crossover point appears for $w \approx 1.8\xi(T)$ as well, with w the width of the wires forming the loop. In the 3D regime, a "giant vortex state" establishes, where superconductivity is concentrated near the sample's outer interface. The vortex is then localized inside the loop's opening.

74.60.Ec, 74.25.Dw, 73.23.-b, 74.20.De, 74.76.-w

Typeset using REVTEX

I. INTRODUCTION

The nucleation of superconductivity in mesoscopic samples has received a renewed interest after the development of nanofabrication techniques, like electron beam lithography. A superconductor is called mesoscopic when the sample size is comparable to the magnetic penetration depth $\lambda(T)$ and the superconducting coherence length $\xi(T)$. In the framework of the Ginzburg-Landau (GL) theory, $\xi(T)$ sets the length scale for spatial variations of the modulus of the superconducting order parameter $|\Psi|$. The pioneering work on mesoscopic superconductors was carried out already in 1962 by Little and Parks¹, who measured the shift of the critical temperature $T_c(H)$ of a (multiply connected) thin-walled Sn microcylinder (a thin-wire "loop") in an axial magnetic field H . The $T_c(H)$ phase boundary showed a periodic component, with the magnetic period corresponding to the penetration of a superconducting flux quantum $\Phi_0 = h/2e$. The Little-Parks oscillations in $T_c(H)$ are a straightforward consequence of the fluxoid quantization constraint, which was predicted by F. London². This condition can be easily understood by integrating the second GL equation

$$\vec{J} = |\Psi|^2 \left(\vec{\nabla} \delta - \frac{2\pi}{\Phi_0} \vec{A} \right) = |\Psi|^2 \vec{v}_s \quad (1)$$

along a closed contour. $J = j/(2e\hbar/m^*)$ is here the normalized current density, v_s is the (normalized) superfluid velocity, and δ is the phase of the complex order parameter $\Psi = |\Psi|e^{i\delta}$. This yields:

$$\oint \frac{\vec{J}}{|\Psi|^2} \cdot d\vec{l} + 2\pi \frac{\Phi}{\Phi_0} = \oint \vec{\nabla} \delta \cdot d\vec{l} = L 2\pi \quad L = \dots, -2, -1, 0, 1, 2, \dots \quad (2)$$

where we used Stokes theorem $\oint \vec{A} \cdot d\vec{l} = \Phi$, with Φ the magnetic flux threading the area inside the contour. In other words, when a non-integer magnetic flux Φ/Φ_0 is applied, a supercurrent J has to be generated in order to fulfill Eq. (2). The integer number L is the phase winding or fluxoid quantum number and gives the number L of flux quanta Φ_0 penetrating the sample. Since, for a cylindrical geometry, the different L states are eigenfunctions of the angular (or orbital) momentum operator as well³, L is often called the angular momentum quantum number. The fluxoid quantization constraint (Eq. (2)) is the equivalent of the Bohr-Sommerfeld quantum condition for Cooper pairs⁴.

A few years later, Saint-James calculated the $T_c(H)$ (or the nucleation magnetic field) of a singly-connected cylinder⁵ (a mesoscopic "disk"). Taking into account the analogy with the situation of a semi-infinite superconducting slab in contact with vacuum⁶, the critical field was called $H_{c3}(T)$ in this case, since superconductivity nucleates initially *near the sample interface*. As we will show further in this paper, a substantial enhancement of the nucleation field, above the $H_{c3}(T)$ for a semi-infinite slab, can be obtained in mesoscopic samples, where the surface-to-volume ratio is large. In such case, surface effects play the role of the bulk effects. Therefore, we will rather use the notation $H_{c3}^*(T)$. For a disk, the limiting value $H_{c3}^*(T) = H_{c3}(T) = 1.69 H_{c2}(T)$ is found as $\Phi \rightarrow \infty$ (or the radius of the disk $\rightarrow \infty$). The field H_{c2} is the upper critical field of a bulk Type II superconductor, at which the Abrikosov vortex lattice is formed.

The $T_c(H)$ phase boundary (or $H_{c3}^*(T)$) of the disk shows, just like for the usual Little-Parks effect in a multiply connected sample (loop), an oscillatory behaviour. In this case,

the oscillation period of $T_c(H)$ is not constant, but slightly decreases as H increases. When moving along $T_c(H)$, superconductivity concentrates more and more near the sample interface as H grows. A giant vortex state is formed: a "normal" core carries L flux quanta, and the 'effective' loop radius increases, resulting in a decrease of the magnetic oscillation period. Here as well, fluxoid quantization (Eq. (2)) is responsible for the oscillations of T_c versus H . An experimental verification of these predictions was carried out later on by Buisson *et al.*⁷ and by Moshchalkov *et al.*⁸.

Currently, many different sample topologies are studied: superconducting networks⁹, antidot systems^{10–12}, samples consisting of sharp corners^{13,14}, etc. With the use of sub-micron Hall probe microscopy¹⁵ for measuring the magnetic response of a superconductor, it has become possible to probe samples deep in the superconducting state¹⁶ (i.e. at temperatures far below T_c). A lot of recent theoretical activities have been devoted to the magnetization and vortex configurations in superconducting disks of different sizes^{14,17}.

Loop structures have also been studied extensively in the past years. A large portion of the theoretical research has been focused on the transition between two different fluxoid states $L \rightarrow L+1$ ^{10,18}, but also experiments, among which susceptibility measurements close to T_c ¹⁹, studies of energy gap spectrum using a single-electron transistor²⁰, and scanning Hall probe measurements on ensembles of mesoscopic Al loops²¹, were carried out.

As it has already been mentioned, the two limiting cases, "thin-wire loop" and "disk", are well understood as far as the nucleation field H_{c3}^* is concerned, but the intermediate case is not. In the early paper from Saint-James and de Gennes⁶, $H_{c3}^*(T)$ has been calculated also for a *film exposed to a parallel magnetic field*, where surface superconductivity can grow along two superconductor/vacuum interfaces. For low magnetic fields, the two surface superconducting sheaths overlap, and, as a result, T_c versus H becomes parabolic, which is characteristic for 2D behaviour. When increasing the field, a crossover to a linear $T_c(H)$ dependence (3D) occurs at $t \approx 2\xi(T)$, with t the film thickness. Shortly after, it was shown that vortices start to nucleate in the film at this dimensional crossover point ($t = 1.8\xi(T)$)²².

The goal of the present paper is to study the phase boundary $T_c(H)$ of loops made of finite width wires (or disks with an opening in the middle, increasing in size). In a Type-II material, superconductivity is expected to be enhanced, with respect to the bulk ($H_{c3}^*(T) > H_{c2}(T)$), both at the external and the internal sample surfaces. As for a film in a parallel field, a 2D-3D dimensional crossover can be anticipated, since the loops may be simply considered as a film, which is bent such that its ends are joined together. We calculate the phase boundary $T_c(H)$ as the ground state solution of the linearized first GL equation with two superconductor/vacuum interfaces. This calculation has been suggested already by several authors^{11,23}, but to the best of our knowledge, it has not been carried out so far. We will show that the $T_c(\Phi)$ of the loops, for low applied magnetic flux (corresponding to the 2D regime), can be described within a simple London picture, where the modulus of the order parameter $|\Psi|$ is spatially constant. As the flux increases, the background depression of $T_c(\Phi)$ is changed from parabolic (2D) to quasi-linear (3D), which indicates the formation of a giant vortex state, where only a surface sheath close to the sample's outer interface is in the superconducting state. Moreover, the oscillation period of $T_c(\Phi)$ becomes identical for the loops as for the full disk, as soon as the transition to 3D behaviour has taken place.

II. THE LINEARIZED GL EQUATION

The linearized first GL equation to be solved in order to find $T_c(H)$ is:

$$\frac{1}{2m^*}(-i\hbar\vec{\nabla} - 2e\vec{A})^2\Psi = |-\alpha|\Psi. \quad (3)$$

This equation is formally identical to the Schrödinger equation for a particle with a charge $2e$ in a magnetic field. Here, at the onset of superconductivity $T \approx T_c(H)$, the nonlinear term $\beta|\Psi|^2\Psi \ll |-\alpha|\Psi$ can be omitted, and demagnetization effects along the field direction do not need to be considered. In this regime, the z -dependence disappears from the equations and therefore an infinitely long cylinder and a disk have identical $T_c(H)$ boundaries. It is further assumed that the penetration depth $\lambda(T) \gg$ sample size, so that $\mu_0\vec{H} = \text{rot}\vec{A}$. It is important to note that H is the *applied magnetic field*, so fields induced by supercurrents J (Eq. (2)) are not taken into account here. The more Type II (the higher κ) the superconducting material is, the larger range of validity our calculations have. The eigenenergies $|-\alpha|$ can be written as:

$$|-\alpha| = \frac{\hbar^2}{2m^* \xi^2(T)} = \frac{\hbar^2}{2m^* \xi^2(0)} \left(1 - \frac{T}{T_{c0}}\right), \quad (4)$$

T_{c0} being the critical temperature in zero magnetic field. From the energy eigenvalues of Eq. (3), the lowest Landau level $|-\alpha_{LLL}(H)|$ is directly related to the highest possible temperature $T_c(H)$, for which superconductivity can exist.

By varying the topology of the sample ("nanostructuring"), the lowest Landau level $|-\alpha_{LLL}|$ can be tuned by confinement of the superconducting condensate. Several examples of this concept can be found in Refs.^{9,24}. Indeed, the solution Ψ of Eq. (3) has to fulfill the Neumann boundary condition

$$(-i\hbar\vec{\nabla} - 2e\vec{A})\Psi|_{\perp,b} = 0, \quad (5)$$

at the sample interfaces b . This requirement guarantees that the supercurrent does not have a component perpendicular to a superconductor/vacuum interface.

For the loop geometries, we choose the cylindrical coordinate system (r, φ) and the gauge $\vec{A} = (\mu_0 H r / 2) \vec{e}_\varphi$, where \vec{e}_φ is the tangential unit vector. The exact solution of the Hamiltonian (Eq. (3)) in cylindrical coordinates takes the following form^{11,23,25,26}:

$$\begin{aligned} \Psi(\Phi, \varphi) &= e^{-iL\varphi} \left(\frac{\Phi}{\Phi_0}\right)^{L/2} \exp\left(-\frac{\Phi}{2\Phi_0}\right) K(-n, L+1, \Phi/\Phi_0) \\ K(a, c, y) &= c_1 M(a, c, y) + c_2 U(a, c, y). \end{aligned} \quad (6)$$

Here $\Phi = \mu_0 H \pi r^2$ is the applied magnetic flux through a circle of radius r . The number n determines the energy eigenvalue. Most generally, the function $K(a, c, y)$ can be any linear combination of the two confluent hypergeometric functions (or Kummer functions) $M(a, c, y)$ and $U(a, c, y)$ ²⁷, but the sample topology puts a constraint on c_1 , c_2 , and n , via the boundary condition (Eq. (5)).

The eigenenergies of Eq. (3) (the Landau levels) are²⁶:

$$| -\alpha | = \frac{2e\hbar\mu_0 H}{2m^*} (2n+1) = \hbar\omega \left(n + \frac{1}{2} \right). \quad (7)$$

where $\omega = 2e\mu_0 H/m^*$ is the cyclotron frequency. *The parameter n depends on L and is not necessarily an integer number*, as we shall see later. With Eq. (4) this can be rewritten as:

$$\frac{r_o^2}{\xi^2(T_c)} = \frac{r_o^2}{\xi^2(0)} \left(1 - \frac{T_c(H)}{T_{c0}} \right) = 4 \left(n + \frac{1}{2} \right) \frac{\Phi}{\Phi_0} = \epsilon(H_{c3}^*) \frac{\Phi}{\Phi_0}, \quad (8)$$

where $\Phi = \mu_0 H \pi r_o^2$ is arbitrarily defined.

The bulk Landau levels can be found when substituting $n = 0, 1, 2, \dots$ in Eqs. (7) and (8), meaning that the lowest level $n = 0$ corresponds to the upper critical field $\mu_0 H_{c2}(T) = \Phi_0 / (2\pi\xi^2(T))$. Let us note that the lowest Landau level ($n = 0$) for a bulk superconductor is degenerate in the phase winding number L , and therefore the eigenfunction can be expanded as $\Psi = \sum c_L \Psi_L$. Interference patterns between the different functions Ψ_L give rise to aperiodic vortex states²⁸.

The boundary condition (Eq. (5)), in cylindrical coordinates, can be simply written as:

$$\left. \frac{\partial |\Psi(r)|}{\partial r} \right|_{r=r_o}, \quad (9)$$

with a superconductor/vacuum interface at a radius r_o . Using $\frac{dM(a,c,y)}{dy} = \frac{a}{c} M(a+1, c+1, y)$ and $\frac{dU(a,c,y)}{dy} = -a U(a+1, c+1, y)$ for the derivatives of the first and second type of Kummer functions, respectively²⁷, and inserting Eq. (6) into Eq. (9) gives:

$$\begin{aligned} c_1 \left[\left(L - \frac{\Phi}{\Phi_0} \right) M(-n, L+1, \Phi/\Phi_0) - \frac{2n}{L+1} \frac{\Phi}{\Phi_0} M(-n+1, L+2, \Phi/\Phi_0) \right] + \\ c_2 \left[\left(L - \frac{\Phi}{\Phi_0} \right) U(-n, L+1, \Phi/\Phi_0) + 2n \frac{\Phi}{\Phi_0} U(-n+1, L+2, \Phi/\Phi_0) \right] \Big|_b = 0, \end{aligned} \quad (10)$$

which has to be solved numerically for each integer value of L , resulting in a set of values $n(L, \Phi)$, with $\Phi = \mu_0 H \pi r_o^2$.

For a disk geometry^{5,7,26}, we have to take $c_2 = 0$ in Eqs. (6) and (10) in order to avoid the divergency of $U(a, c, y \rightarrow 0) = \infty$ at the origin. Selecting the lowest Landau level at each value Φ , one ends up with a cusp-like $T_c(H)$ phase boundary⁵, which is composed of values $n < 0$ in Eq. (7), thus leading to $H_{c3}^*(T) > H_{c2}(T)$. A similar calculation was performed for a single circular microhole in a plane film ("antidot")¹¹, where $c_1 = 0$ in Eqs. (6) and (10), since $M(a, c, y \rightarrow \infty) = \infty$. Here as well, the lowest Landau level consists of solutions with $n < 0$. At each cusp in $T_c(\Phi)$, the system makes a transition $L \rightarrow L \pm 1$, i.e. a vortex enters or is removed from the sample.

The loops we are currently studying have two superconducting/vacuum interfaces, one at the outer radius r_o , and one at the inner radius r_i . Consequently, the boundary condition (Eq. (10)) has to be fulfilled at both r_o , and r_i . As a result, we have a system of two equations and two variables n and c_2 ($c_1 = 1$ is chosen), which we solved for different values of $x = r_i/r_o$. *In the rest of the paper we will define $\Phi = \mu_0 H \pi r_o^2$, where r_o always means the outer loop radius.*

III. THE LONDON LIMIT

The usual description of the Little-Parks effect^{4,29} is given in terms of the London limit, where $|\Psi|$ is spatially constant. This approximation, of course, is valid when the wire, forming the loop, is very thin ($x \approx 1$), or when we define the loop aspect ratio z as

$$z = \frac{r_o - r_i}{r_o + r_i} = \frac{1 - x}{1 + x}, \quad (11)$$

this condition implies $z \ll 1$.

The solution of the linearized GL equation (Eq. (3)) becomes³⁰:

$$\frac{r_m^2}{\xi^2(T_c)} = \frac{r_m^2}{\xi^2(0)} \left(1 - \frac{T_c(H)}{T_{c0}}\right) = \left(\frac{\Phi_m}{\Phi_0}\right)^2 (1 + z^2) - 2L \frac{\Phi_m}{\Phi_0} + \frac{L^2}{2z} \ln\left(\frac{1+z}{1-z}\right), \quad (12)$$

with $\Phi_m = \mu_0 H \pi r_m^2$, r_m is the mean radius of the loop. Note that this definition of flux Φ_m is different from Φ in the previous section. The lowest eigenvalues are obtained when L is the integer number closest to $-2(\Phi_m/\Phi_0)z/\ln x$. We will further compare this equation with our more exact results, calculated from the scheme presented in the previous section.

Since in the original paper by Groff and Parks³⁰, thin-wire loops ($z \ll 1$) were investigated, the logarithm was expanded in a Taylor series, which gives, up to the order z^2 :

$$\frac{r_m^2}{\xi^2(T_c)} = \frac{r_m^2}{\xi^2(0)} \left(1 - \frac{T_c(H)}{T_{c0}}\right) = \left(L - \frac{\Phi_m}{\Phi_0}\right)^2 + \frac{4}{3} z^2 \left(\frac{\Phi_m}{\Phi_0}\right)^2. \quad (13)$$

The first term on the right hand side of Eq. (13) is the periodic part of the T_c reduction (i.e. the Little-Parks effect), while the second term is a monotonic parabolic background, which is identical to the $T_c(H)$ expression for a plane film of thickness $t = 2zr_m$ in a parallel magnetic field⁴. In Ref.³⁰, a substitution is performed, which splits the right hand side of Eq. (12) in a periodic term and a monotonic background T_c . The latter becomes:

$$\frac{r_m^2}{\xi^2(T_c)} = (1 + z^2) \left\{ \left(\frac{1 + z^2}{2z} \right) \ln\left(\frac{1+z}{1-z}\right) - 1 \right\} \left(\frac{\Phi_m}{\Phi_0}\right)^2, \quad (14)$$

which is parabolic with Φ_m . This substitution is only valid for thin-wire loops, and Eq. (14) transforms of course into the last term of Eq. (13) for $z \ll 1$.

IV. RESULTS

Fig. 1 shows the Landau level scheme (dashed lines) calculated from Eqs. (8), and (10) for loops with a different inner radius $x = r_i/r_o$ (a) $x = 0.1$, (b) $x = 0.3$, (c) $x = 0.5$, (d) $x = 0.7$, and (e) $x = 0.9$. The applied magnetic flux $\Phi = \mu_0 H \pi r_o^2$ is defined with respect to the outer sample area. The $T_c(H)$ boundary (or $|\alpha_{LLL}(H)|$) is composed of Ψ solutions with a different phase winding number L and is drawn as a solid cusp-like line in Fig. 1. At $\Phi \approx 0$, the state with $L = 0$ is formed at $T_c(H)$ and one by one, consecutive flux quanta L enter the loop as the magnetic field increases. Each state L approximately has a parabolic dependence $|\alpha(H)|$, close to $T_c(H)$. Like for the disk^{16,23}, where $\Phi \approx \Phi_0 (L + L^{1/2})$, we

have here as well $L\Phi_0 \leq \Phi$, indicating the overall diamagnetic response of the sample. As x increases, the oscillations in $T_c(\Phi)$ change from cusp-like, to very pronounced local extrema for $x = 0.9$. In the limit of vanishing wire width ($x \rightarrow 1$), L is the integer closest to Φ_m/Φ_0 , and therefore the response of the loop is alternating between diamagnetic and paramagnetic, as the flux varies.

The solid and dotted straight lines in Fig. 1 are the bulk upper critical field $H_{c2}(T)$ and the surface critical field $H_{c3}(T)$ for a semi-infinite slab, respectively. In these units the slopes of the curves (see Eq. (8)) are $\epsilon = 2$ for H_{c2} (substitute $n = 0$ in Eq. (8)) and $\epsilon = 2/1.69$ for H_{c3} . The ratio $\eta = \epsilon(H_{c2})/\epsilon(H_{c3}) = 1.69$ corresponds then to the enhancement factor $H_{c3}(T)/H_{c2}(T)$ at a constant temperature. For the loops we are studying here $\eta = \epsilon(H_{c2})/\epsilon(H_{c3}^*)$ is no longer a constant, but varies with the magnetic field.

The energy levels below the H_{c2} line (solid straight line in Fig. 1) could be found by fixing a certain L , and solving Eq. (10) for a small Φ , until a set (n, c_2) is found with $n < 0$. These values were always put in as starting values for a slightly higher Φ . A trivial solution of Eq. (10) is obtained for $n = 0, 1, 2, \dots$. Both confluent hypergeometric functions reduce to $M(-N, L+1, \Phi/\Phi_0) = 1$ and $U(-N, L+1, \Phi/\Phi_0) = 1$, and thus $c_2 = -c_1$. Inserting this into Eq. (6) gives $\Psi(\Phi, \varphi) = 0$ everywhere. With this method, we were able to find solutions with $n < 0$ numerically. Note that the lowest Landau level always has a lower energy $|- \alpha(\Phi)|$ than for a semi-infinite superconducting slab, which implies $H_{c3}^*(T) > H_{c3}(T)$.

The dash-dotted curve in Fig. 1 gives the result obtained with the London limit³⁰ (see Eq. (12)). In Fig. 1a ($x = 0.1$) the deviation from the exact solution of Eq. (3) appears already for $L \geq 1$. For low flux, the result from Eq. (12), has clearly higher energy $|- \alpha|$ than the surface critical field $H_{c3}(T)$. At $\Phi \approx 7\Phi_0$, this curve even crosses the bulk $H_{c2}(T)$ line, which is clearly unphysical. For $x = 0.3$ (Fig. 1b) the London limit is valid up to $\Phi \approx 4\Phi_0$, up to $\Phi \approx 8\Phi_0$ for $x = 0.5$ (Fig. 1c), and for $x = 0.7$ (Fig. 1d) it is a good approximation in the whole flux interval of our calculations. Finally, for $x = 0.9$ (Fig. 1e) the assumption of a spatially constant $|\Psi|$ gives a $T_c(\Phi)$, which can not be distinguished from the exact solution of Eq. (3).

In Fig. 1a ($x = 0.1$) the background depression of T_c is *quasi-linear*, just like for the case of a filled disk, for $x = 0.3$ (Fig. 1b) $T_c(H)$ has a rather *parabolic* background for flux $\Phi \lesssim 7\Phi_0$, and becomes quasi-linear at higher flux. This becomes more clear for $x = 0.5$ (Fig. 1c). Here, the crossover point from parabolic to quasi-linear appears at about $\Phi \approx 14\Phi_0$. In Figs. 1d and 1e finally ($x = 0.7, x = 0.9$), the background is parabolic in the entire flux regime and can be very accurately described by Eq. (14). Simultaneously, as x increases, the cusps in $T_c(H)$ become more and more pronounced, until the usual Little-Parks effect is recovered for $x = 0.9$ (see Eq. (13)), where sharp local minima and clear maxima in $T_c(H)$ are seen.

V. DISCUSSION

In order to study the spatial variation of the order parameter $|\Psi|$, we will use Abrikosov's definition of the flatness parameter $\beta_A = <|\Psi|^4> / <|\Psi|^2>^2$, where the brackets indicate the average over the actual sample area³¹ (not including the middle opening). Abrikosov introduced this parameter β_A in order to find the most favorable order parameter distribution, in a bulk system, near the H_{c2} line. In this language, $\beta_A = 1$ means a completely flat profile

of $|\Psi|$, corresponding to the London limit. For comparison, we mention that $\beta_A = 1.16$ for a triangular Abrikosov vortex lattice.

In Fig. 2 we plot the modulus of the order parameter $|\Psi|$ for the case $x = 0.1$, at $\Phi = 9\Phi_0$, for the states a) $L = 2$, b) $L = 3$, c) $L = 4$, d) $L = 5$, and e) $L = 6$. The $|\Psi|$ values have been normalized to 1 at the sample's outer interface $r = r_o$. The dark area is the region outside the sample. The maximum in $|\Psi|$ for $L = 2$ lies at $r \approx (r_i + r_o)/2$, and gradually shifts to the outer sample edge as $L \rightarrow 6$, which is the ground state solution of Eq. (3). The spatial modulation of $|\Psi|$ is considerable ($\beta_A > 1.16$) for all $|\Psi|$ patterns shown here. At $T = T_c(\Phi)$ (Fig. 2e), ($L = 6$, $\beta_A = 1.59$) the sample is in the "giant vortex state", with a normal core containing 6 flux quanta Φ_0 , and a surface superconducting sheath at the outer sample edge.

The $|\Psi|$ profiles for a loop with a larger inner radius ($x = 0.5$) are shown in Fig. 3. Here as well, we have chosen $\Phi = 9\Phi_0$, and the same normalization $|\Psi(r_o)| = 1$. a) $L = 2$, b) $L = 3$, c) $L = 4$, d) $L = 5$, and e) $L = 6$. For $L = 2$ (Fig. 3a), $|\Psi|$ has a maximum at $r = r_i$. For higher L the order parameter distribution flattens until it reaches $\beta_A = 1.06$ for $L = 4$. Then, for the ground state energy ($L = 5$) (Fig. 3d), the maximum in $|\Psi|$ moves outward, but we should notice that for this state $\beta_A = 1.01$ only, which means that superconductivity nucleates in a quasi-uniform way. Indeed, the exact $T_c(\Phi)$ and the London limit result are still very close to each other at $\Phi = 9\Phi_0$ (see Fig. 1c). Although multiple flux quanta L are threading the middle opening of the loop, we can not, in the strict sense, speak about a giant vortex state here. First of all, there is no real 'normal core' within the sample area, and secondly we are not dealing with a surface superconducting state in this case. The surface-to-volume ratio is so large that the whole sample area becomes superconducting at once. On the contrary, for the disk, strong spatial gradients of $|\Psi|$ are responsible for the spontaneous breaking of superconductivity in the giant vortex core, while only a surface sheath is superconducting.

It is worth noting that for all of the states shown in Fig. 2 ($x = 0.1$), the width of the wire $w = r_o - r_i = (1 - x)r_o > 2.7\xi(T)$ (see also Fig. 1a), while for the loop with $x = 0.5$ the different L states from Fig. 3 correspond to $w < 2.1\xi(T)$ (see also Fig. 1c). At this point we want to remind that in a thin film of thickness t in a parallel field H , a dimensional crossover is found at $t = 1.84\xi(T)$. For low fields (high ξ) $T_c(H)$ is parabolic (2D), and for higher fields vortices start penetrating the film and consequently $T_c(H)$ becomes linear (3D)²². In Figs. 1a, b, and c the small arrow indicates the point on the phase diagram $T_c(\Phi)$ where $w = 1.84\xi(T)$. For loops with larger x this point lies outside the flux regime of the calculations. For the loops as well, the dimensional transition shows up approximately at this point, although the vortices are not penetrating the sample area in the 3D regime. Instead, the middle loop opening contains an integer number of flux quanta $L\Phi_0$. In the present case, the 2D-3D crossover roughly occurs at the value Φ where the London limit result (Eq. (12)) fails to describe the exact $T_c(\Phi)$.

In order to compare the flux periodicity of $T_c(\Phi)$, we have replotted, in Fig. 4, the lowest energy levels of Fig. 1 as $\eta^{-1} = \epsilon(H_{c3}^*)/\epsilon(H_{c2})$, which is the inverse enhancement factor at a constant temperature. In this representation, the dotted horizontal line at $\eta^{-1} = 0.59$ corresponds to the surface critical field line $H_{c3}(T)$. The nucleation field of a disk $H_{c3}^*(T) > 1.69 H_{c2}(T)$ (i.e. $\eta > 1.69$), and for a circular microhole in an infinite film ("antidot")¹¹ $H_{c3}^*(T) < 1.69 H_{c2}(T)$ ($\eta < 1.69$). As Φ grows (the radius goes to infinity) the $H_{c3}^*(T)$ of

both the disk and the antidot approaches the $H_{c3}(T)$ line.

At this point, we would like to come back to the explanation why the notation $H_{c3}^*(T)$ was used for the nucleation field. For a thin film (thickness t) with the field H applied parallel to the surfaces, $T_c(H)$ is found from the second term of Eq. (13). With $t = 2zr_m$ and $\mu_0 H_{c2} = \Phi_0/(2\pi\xi^2(T))$, this becomes

$$H_{c3}^*(T) = \frac{\sqrt{12}\xi(T)}{t} H_{c2}(T) = 2.04 \frac{\xi(T)}{t} H_{c3}(T), \quad (15)$$

which implies directly $H_{c3}^*(T) > H_{c3}(T)$ for very thin films $t < 2.04\xi(T)^{32}$. Note that $t = w \approx 2.04\xi(T)$ is very close to the 2D-3D crossover point in films and in loops. Of course, the possibility for nucleation fields $H_{c3}^* > H_{c3}$ is not very special, but it still creates a lot of confusion. In thin films, for example, the critical field $H_{c3}^*(T)$ is often denoted as $H_{c2,\perp}$ in a perpendicular magnetic field, and $H_{c2,\parallel}$ in a parallel field, which would mean $H_{c2,\parallel}(T) > H_{c3}(T)$ for $t < 2.04\xi(T)$ (Eq. (15)). Van Gelder studied the H_{c3}^* of a semi-infinite film which is bent over a certain angle (a "wedge") and even called it H_{c4} , since it exceeds H_{c3} at small angles³³. Since this is just a finite size effect and indeed no new nucleation mechanism is involved, the existence of a $H_{c4} > H_{c3}$ was called a misinterpretation by Fink³². For all these reasons, it is safe to use the notation H_{c3}^* for the nucleation field. Enhancing the nucleation field $H_{c3}^*(T)$ can be realized by confining the superconducting condensate in a mesoscopic sample. The smaller the sample size, the lower the Landau level $|- \alpha_{LLL}(H)|$ becomes, when Neumann boundary conditions (Eq. (5)) are imposed. The idea of having $H_{c3}^* > H_{c3} = 1.69 H_{c2}$ was used to explain anomalously high values of H_{c3}^* and attribute this to the existence of small surface irregularities (of the order of ξ), impurities, grain boundaries or concentration gradients near the interface³⁴.

For all the loops we study here, the presence of the outer sample interface automatically implies that $H_{c3}^*(T) > H_{c3}(T)$ is enhanced ($\eta > 1.69$), with respect to the case of a flat superconductor-vacuum interface. For loops with a small x , the $T_c(\Phi)$ boundary very rapidly collapses with the $T_c(\Phi)$ of the dot (for $\Phi > 4\Phi_0$) (η becomes the same). Since both the flux periodicity and the background depression of T_c become identical to the disk, a giant vortex state can be anticipated for the loop as well. The presence of the opening in the sample is not relevant for the giant vortex formation in the high flux regime. Indeed, for the ground state level of Fig. 2 ($x = 0.1$, $L = 6$), which is marked with a circle in Fig. 4, the giant vortex state has clearly been formed already. On the contrary, for $x = 0.5$, $L = 5$, at $\Phi = 9\Phi_0$, marked with a square in Fig. 4, superconductivity nucleates in a uniform way ($\beta_A = 1.01$) (see Fig. 3).

The formation of the giant vortex state at high Φ can be understood when writing the GL free energy^{4,29}

$$F = F_n + S \langle \alpha |\Psi|^2 \rangle + S \frac{\hbar^2}{2m^*} \left\langle \left(-i\vec{\nabla} - \frac{2\pi}{\Phi_0} \vec{A} \right) \Psi \right\rangle^2 + \dots, \quad (16)$$

with the sum of the last two terms vanishing at the phase boundary $T_c(H)$, where $\Psi \rightarrow 0$. F_n is the free energy of the system in the normal state. The notation $\langle \rangle$ denotes the average over the sample area S , and $|\alpha| = \hbar^2/2m^*\xi^2(T)$. This yields (see Eq. (1)):

$$\frac{1}{\xi^2(T)} = \frac{\langle |\Psi|^2 \vec{v}_s^2 \rangle + \langle (\vec{\nabla}|\Psi|)^2 \rangle}{\langle |\Psi|^2 \rangle} \quad (17)$$

The solutions from Eq. (6) which fulfill the boundary conditions (Eq. (5)) in $r = r_i$ and $r = r_o$ need to be inserted in this equation, and v_s is determined from Eq. (2). A fast calculation shows that the relative contribution from spatial gradients (the second term in the numerator of Eq. (17)) is 47 % for the lowest level of Fig. 2e ($x = 0.1$, $L = 6$), while it is less than 4 % for the ground state of Fig. 3d ($x = 0.5$, $L = 5$). The energetically most favourable balance between these two contributions is strongly affected by the boundary conditions (Eq. 5). In thin-wire loops, for example, bending of $|\Psi|$ on a scale smaller than the coherence length ξ will result in a large contribution of $\langle (\vec{\nabla}|\Psi|)^2 \rangle$. Therefore, the T_c reduction is only determined by the averaged supercurrent kinetic energy $\langle |\Psi|^2 \vec{v}_s^2 \rangle$ in this case, which is equivalent to the London limit.

An examination of the supercurrent flow profiles shows that, as in the case of a filled disk, there is a paramagnetic contribution close to the sample center for $L \neq 0$, while near the outer sample interface diamagnetic currents are flowing. The supercurrent density J can be obtained by inserting the general solution (Eq. (6)) in the second GL equation (Eq. (2)):

$$\vec{J}(L, \Phi) = |\Psi|^2 \vec{v}_s \propto \left(L - \frac{\Phi}{\Phi_0}\right) \left(\frac{\Phi}{\Phi_0}\right)^{L-\frac{1}{2}} \exp\left(-\frac{\Phi}{\Phi_0}\right) [K(-N, L+1, \Phi/\Phi_0)]^2 \vec{e}_\varphi \quad (18)$$

At a radius r , corresponding to integer flux quanta $\Phi = L \Phi_0$ the current orientation changes sign. It can happen, however, that the switching radius $r < r_i$, lies inside the middle opening. For the state $L = 0$ there are only diamagnetic currents. In contrast to this, for example, for a loop with $x = 0.5$, the states $L = 2$ (Fig. 3a) and $L = 3$ (Fig. 3b) do not carry paramagnetic currents at $\Phi = 9 \Phi_0$. At the ground state level ($L = 5$) (Fig. 3d), which is very close to the London limit solution, $J \propto v_s \propto (L - \Phi/\Phi_0)/r$ (Eq. (2)). This is shown in the right inset of Fig. 4, where the supercurrent has been normalized to -1 at the outer radius r_o . For the loop with $x = 0.1$ (see Fig. 2e), in the ground state $L = 6$, the dominating diamagnetic supercurrents are flowing in the vicinity of $r = r_o$, the currents are paramagnetic for slightly lower r , and J is vanishing in the core of the sample $r_i < r < r_o/3$ (left inset of Fig. 4).

As a last point, we discuss now the periodicity $\Delta\Phi$ of $T_c(\Phi)$, for the different L states in the loops. These results are shown in Fig. 5. For the disk, the first cusp in $T_c(\Phi)$, where L goes from $0 \rightarrow 1$, occurs at $\Phi = 1.92 \Phi_0$, so $\Delta\Phi(L=0) = 3.85 \Phi_0$. The period $\Delta\Phi$ goes down for increasing L , until it reaches the asymptotic limit⁷:

$$\Delta\Phi = \Phi_0 \left(1 + (2\eta\Phi/\Phi_0)^{-1/2}\right) \quad (19)$$

Since η is decreasing with Φ , $\Delta\Phi$ is a weakly decreasing function of L , at high Φ . The symbols in Fig. 5 correspond to the period $\Delta\Phi$ in units of Φ_0 for the different L states. Since at the highest Φ , $T_c(\Phi)$ is calculated in steps of $\approx 0.07 \Phi_0$, the error on $\Delta\Phi$ is of this order. The filled squares are the periods for the filled disk. The periodicity of $T_c(\Phi)$ in the case of loops behaves differently: for $x = 0.1$ (filled up-triangles in Fig. 5) $\Delta\Phi(L=1) = 1.82 \Phi_0$ is larger than for the filled disk, then $\Delta\Phi(L=2)$ jumps below the corresponding value for the disk, and for higher $L \geq 3$, the period $\Delta\Phi$ matches with the disk behaviour. Consequently, the giant vortex state builds up for $L \geq 3$, i.e. $\Phi \gtrsim 5 \Phi_0$. A similar analysis can be carried out for a loop with $x = 0.5$ (filled down-triangles in Fig. 5). For low L , $\Delta\Phi \approx 1.8 \Phi_0$, then $\Delta\Phi(L)$ decreases substantially below the value for the filled disk, before increasing again, until the same period $\Delta\Phi(L)$ is reached for $L \geq 12$. The loop is in the giant vortex state

when $\Phi \gtrsim 17 \Phi_0$. For loops made of even thinner wires ($x = 0.7$ and $x = 0.9$) (open symbols in Fig. 5), $T_c(\Phi)$ stays periodic up to $L = 13$. The constant period $\Delta\Phi$ corresponds to $\Delta\Phi_m = ((1+x)/2)^2 \Delta\Phi = 1 \Phi_0$, as it should be in the London limit for $x \rightarrow 1$, according to Eq. (13).

In summary, we have solved the linearized GL equation for loops of different wire width, with Neumann boundary conditions at both the outer and the inner loop radius. The critical fields $H_{c3}^*(T)$ are always above the $H_{c3}(T) = 1.69 H_{c2}(T)$, the surface critical field for a semi-infinite superconducting slab in contact with vacuum. The ratio $H_{c3}^*(T)/H_{c2}(T)$ increases when the size of the middle opening grows, i.e. in a sample topology with a large surface-to-volume ratio the nucleation field is strongly enhanced. Depending on the ratio inner to outer radius r_i/r_o of the loops, and on the applied magnetic flux, $T_c(\Phi)$ shows a different behaviour: in thin-wire loops, the background of T_c is parabolic (characteristic for 2D behaviour) and the Little-Parks $T_c(\Phi)$ oscillations are perfectly periodic. This behaviour can be described in the London limit. For loops with only a very small opening, the period of the $T_c(\Phi)$ oscillations is decreasing with Φ and the background T_c reduction is quasi-linear (3D regime, e.g., like for a disk). Intermediate loops (for instance $r_i/r_o = 0.5$) show a 2D-3D cross-over between the two regimes at a certain applied flux Φ (corresponding to $w = r_o - r_i = (1-x) r_o \approx 2 \xi(T)$), similar to the dimensional transition in thin films subjected to a parallel field. As soon the 3D regime is reached, a giant vortex state is created, where only a sheath close to the sample's outer interface is superconducting. The opening in the middle of the loop does not play a role anymore: $T_c(\Phi)$ for the loop and for the disk become identical.

ACKNOWLEDGMENTS

The authors wish to thank H. J. Fink, T. Puig, J. G. Rodrigo, J. T. Devreese, V. M. Fomin, K. Temst, and J. O. Indekeu for stimulating discussions. This work has been supported by the Belgian IUAP, the Flemish GOA and FWO-programmes, and by the ESF programme VORTEX.

* e-mail: Vital.Bruyndoncx@fys.kuleuven.ac.be

REFERENCES

- ¹ W.A. Little and R.D. Parks, Phys. Rev. Lett. **9**, 9 (1962); R.D. Parks and W.A. Little, Phys. Rev. **133**, A97 (1964).
- ² F. London, *Superfluids*, John Wiley & Sons, Inc., New York, 1950.
- ³ M. Daumens, C. Meyers, and A. Buzdin, Physics Letters A **248**, 445 (1998).
- ⁴ M. Tinkham, *Introduction to Superconductivity*, McGraw Hill, New York (1975).
- ⁵ D. Saint-James, Phys. Lett. **15**, 13 (1965).
- ⁶ D. Saint-James and P.-G. de Gennes, Phys. Lett. **7**, 306 (1963).
- ⁷ O. Buisson, P. Gandit, R. Rammal, Y. Y. Wang, and B. Pannetier, Phys. Lett. A **150**, 36 (1990).
- ⁸ V. V. Moshchalkov, L. Gielen, C. Strunk, R. Jonckheere, X. Qiu, C. Van Haesendonck, and Y. Bruynseraede, Nature **373**, 319 (1995).
- ⁹ B. Pannetier, in *Quantum coherence in mesoscopic systems*, edited by B. Kramer, (Plenum Press, New York, 1991) and references therein.
- ¹⁰ A. Bezryadin, A. Buzdin, and B. Pannetier, Phys. Rev. B **51**, 3718 (1995).
- ¹¹ A. Bezryadin and B. Pannetier, J. Low Temp. Phys. **98**, 251 (1995); A. Bezryadin, A. Buzdin, and B. Pannetier, Phys. Lett. A **195**, 373 (1994).
- ¹² V. V. Moshchalkov, M. Baert, V. V. Metlushko, E. Rosseel, M. J. Van Bael, K. Temst, R. Jonckheere, and Y. Bruynseraede, Phys. Rev. B **54**, 7385 (1996).
- ¹³ V. M. Fomin, J. T. Devreese, and V. V. Moshchalkov, Europhys. Lett. **42**, 553 (1998) + erratum in Europhys. Lett. **46**, 118 (1999); V. M. Fomin, V. R. Misko, J. T. Devreese, and V. V. Moshchalkov, Phys. Rev. B **58**, 11703 (1998); V. Bruyndoncx, J. G. Rodrigo, T. Puig, L. Van Look, V. V. Moshchalkov, and R. Jonckheere, Phys. Rev. B **60**, (1999); H. T. Jadallah, J. Rubinstein, and P. Sternberg, Phys. Rev. Lett. **82**, 2935 (1999); V. A. Schweigert and F. M. Peeters, Phys. Rev. B **60**, R..... (1999).
- ¹⁴ V. A. Schweigert and F. M. Peeters, Phys. Rev. B **57**, 13817 (1998).
- ¹⁵ A. K. Geim, S. V. Dubonos, J. G. S. Lok, I. V. Grigorieva, J. C. Maan, L. Theil Hansen, and P. E. Lindelof, Appl. Phys. Lett. **71**, 2379 (1997).
- ¹⁶ A. K. Geim, I. V. Grigorieva, S. V. Dubonos, J. G. S. Lok, J. C. Maan, A. E. Filippov, and F. M. Peeters, Nature **390**, 259 (1997); A. K. Geim, S. V. Dubonos, J. G. S. Lok, M. Henini, and J. C. Maan, Nature **396**, 144 (1998).
- ¹⁷ A. I. Buzdin and J. P. Brison, Physics Letters A **196**, 267 (1994); P. S. Deo, V. A. Schweigert, F. M. Peeters, and A. K. Geim, Phys. Rev. Lett. **79**, 4653 (1997); V. A. Schweigert, F. M. Peeters, and P. S. Deo, Phys. Rev. Lett. **81**, 2783 (1998); J. J. Palacios, Phys. Rev. B **58**, R5948 (1998); J. J. Palacios, Physica B **256-258**, 610 (1998); E. Akkermans and K. Mallick, cond-mat/9812275 (16 Dec 1998); G. M. Braverman, S. A. Gredeskul, and Y. Avishai, cond-mat/9901040 (7 Jan 1999).
- ¹⁸ J. Berger and J. Rubinstein, Phys. Rev. Lett. **75**, 320 (1995); E. M. Horane, J. I. Castro, G. C. Buscaglia, and A. López, Phys. Rev. B **53**, 9296 (1996); J. Berger and J. Rubinstein, Phys. Rev. B **59**, 8896 (1999).
- ¹⁹ X. Zhang and J. C. Price, Phys. Rev. B **55**, 3128 (1997).
- ²⁰ H. Sato, S. Katsumoto, and Y. Iye, Physica B **249-251**, 453 (1998).
- ²¹ D. Davidovic, S. Kumar, D. H. Reich, J. Siegel, S. B. Field, R. C. Tiberio, R. Hey, and K. Ploog, Phys. Rev. Lett. **76**, 815 (1996); D. Davidovic, S. Kumar, D. H. Reich, J. Siegel, S. B. Field, R. C. Tiberio, R. Hey, and K. Ploog, Phys. Rev. B **55**, 6518 (1997).

²² H. J. Fink, Phys. Rev. **177**, 732 (1969); H. A. Schultens, Z. Physik **232**, 430 (1970).

²³ R. Benoist and W. Zwerger, Z. Phys. B **103**, 377 (1997).

²⁴ V. V. Moshchalkov *et al.*, Physica Scripta **T55**, 168 (1994); for a recent review, see V. V. Moshchalkov, V. Bruyndoncx, L. Van Look, M. J. Van Bael, and Y. Bruynseraede, in *Handbook of Nanostructured Materials and Nanotechnology*, edited by H. S. Nalwa, Volume 3, Chapter 9, (Academic Press, San Diego, 1999) and references therein.

²⁵ R. B. Dingle, Proc. R. Soc. London, Ser. A **211**, 500 (1952).

²⁶ V. V. Moshchalkov, X. G. Qiu, and V. Bruyndoncx, Phys. Rev. B **55**, 11793 (1997).

²⁷ M. Abramowitz and I. A. Stegun, *Handbook of Mathematical Functions*, Dover Publications, Inc., New York, 1970.

²⁸ V. V. Moshchalkov, M. Dhallé, and Y. Bruynseraede, Physica C **207**, 307 (1993).

²⁹ P.-G. de Gennes, *Superconductivity of Metals and Alloys*, Benjamin, New York (1966).

³⁰ R. P. Groff and R. D. Parks, Phys. Rev. **176**, 567 (1968).

³¹ A. A. Abrikosov, *Fundamentals of the Theory of Metals*, North-Holland, Amsterdam (1988).

³² A. Rothwarf, Phys. Letters **24A**, 343 (1967); H. J. Fink, Phys. Rev. **177**, 1017 (1969).

³³ A. P. van Gelder, Phys. Rev. Lett. **20**, 1435 (1968).

³⁴ J. Lowell, Phil. Mag. **16**, 581 (1967) and references therein; W. C. H. Joiner, Phil. Mag. **166**, 807 (1969) and references therein.

FIGURES

FIG. 1. Calculated energy level scheme (dashed lines) for a superconducting loop with different ratio of inner to outer radius $x = r_i/r_o$: a) $x = 0.1$, b) $x = 0.3$, c) $x = 0.5$, d) $x = 0.7$, and e) $x = 0.9$. The lowest level for each magnetic flux Φ/Φ_0 corresponds to the highest possible temperature $T_c(H)$ for which superconductivity can exist. A state with phase winding number $L = 0$ is formed at $T_c(\Phi \approx 0)$, and at each cusp in $T_c(H)$ the system makes a transition $L \rightarrow L + 1$, indicating the entrance of an extra vortex. The solid and dotted lines correspond to $H_{c2}(T)$ and $H_{c3}(T)$, respectively.

FIG. 2. Order parameter distribution $|\Psi|$ for $x = r_i/r_o = 0.1$, at a fixed $\Phi = 9\Phi_0$. a) $L = 2$, b) $L = 3$, c) $L = 4$, d) $L = 5$, and e) $L = 6$. The latter ($L = 6$) corresponds to the ground state level $| -\alpha_{LLL}(9\Phi_0) |$, where the sample is in the giant vortex state.

FIG. 3. Order parameter distribution $|\Psi|$ for $x = 0.5$, at a fixed $\Phi = 9\Phi_0$. a) $L = 2$, b) $L = 3$, c) $L = 4$, d) $L = 5$, and e) $L = 6$. The state with $L = 5$ is only slightly modulated ($|\Psi| \approx \text{constant}$: $\beta_A = 1.01$) and corresponds to the ground state level $| -\alpha_{LLL}(9\Phi_0) |$.

FIG. 4. Inverse enhancement factor $\eta^{-1} = \epsilon(H_{c3}^*)/\epsilon(H_{c2})$ for loops with different aspect ratio, compared to the case of a disk and an antidot. The horizontal dashed line at $\eta^{-1} = 0.59 = 1/1.69$ corresponds to $H_{c3}(T)/H_{c2}(T) = 1.69$ for a plane superconductor/vacuum boundary. The insets show the supercurrent J profiles for the ground states at $\Phi = 9\Phi_0$ for $x = r_i/r_o = 0.1$ (left) and $x = 0.5$ (right). These are obtained from Eq. (18) and are normalized to -1 at the outer radius $r = r_o$. The corresponding $|\Psi|$ profiles are plotted in Fig. 2e, and Fig. 3d, respectively.

FIG. 5. The period $\Delta\Phi$ of the phase boundary $T_c(\Phi)$ in units of the flux quantum Φ_0 as a function of the phase winding number L . The data, for several of the loops is shown as a symbol, and is compared to the period in a filled disk (filled square). The interconnecting lines are only a guide to the eye.

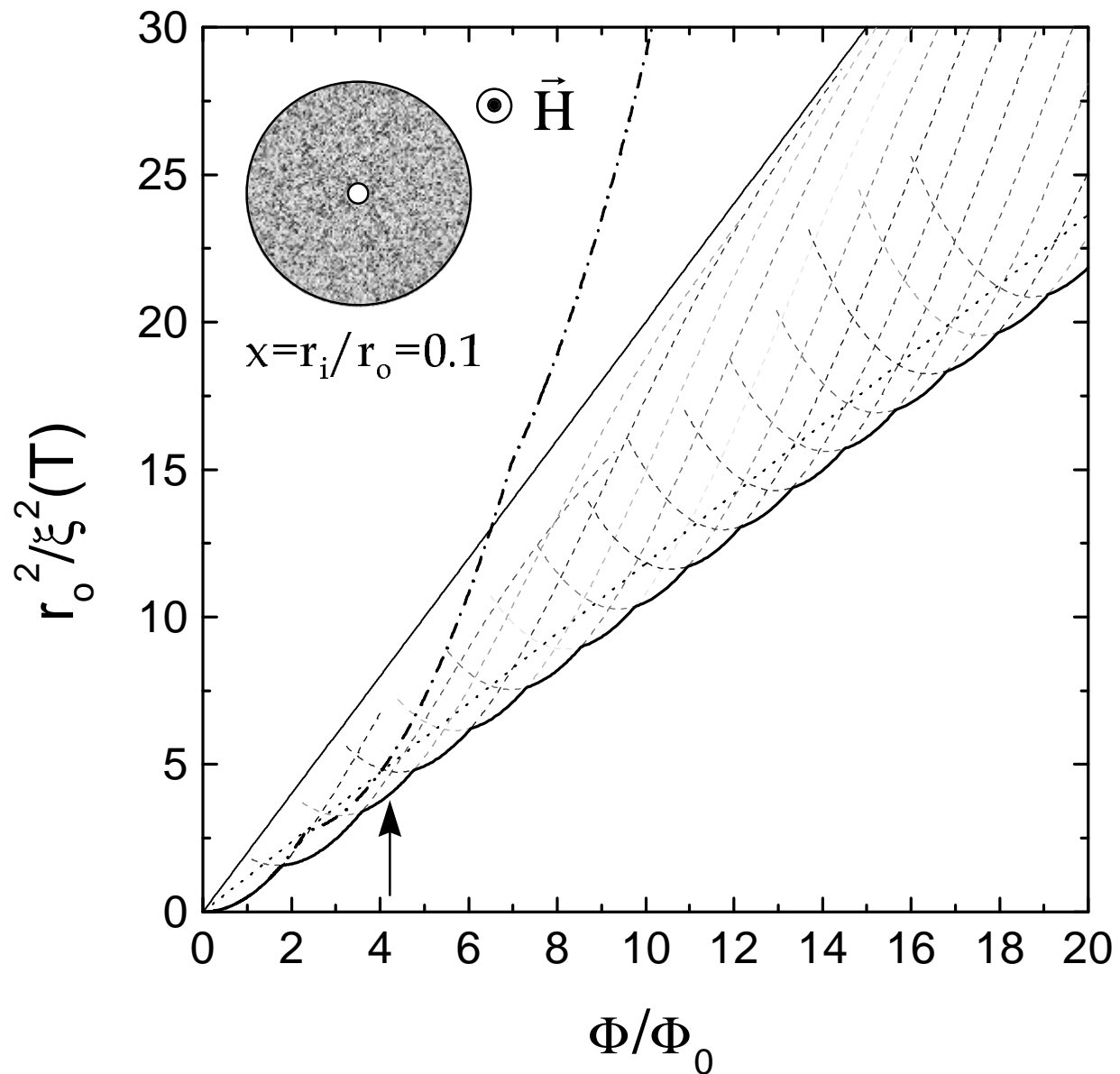


Fig. 1a
Bruyndoncx et al.

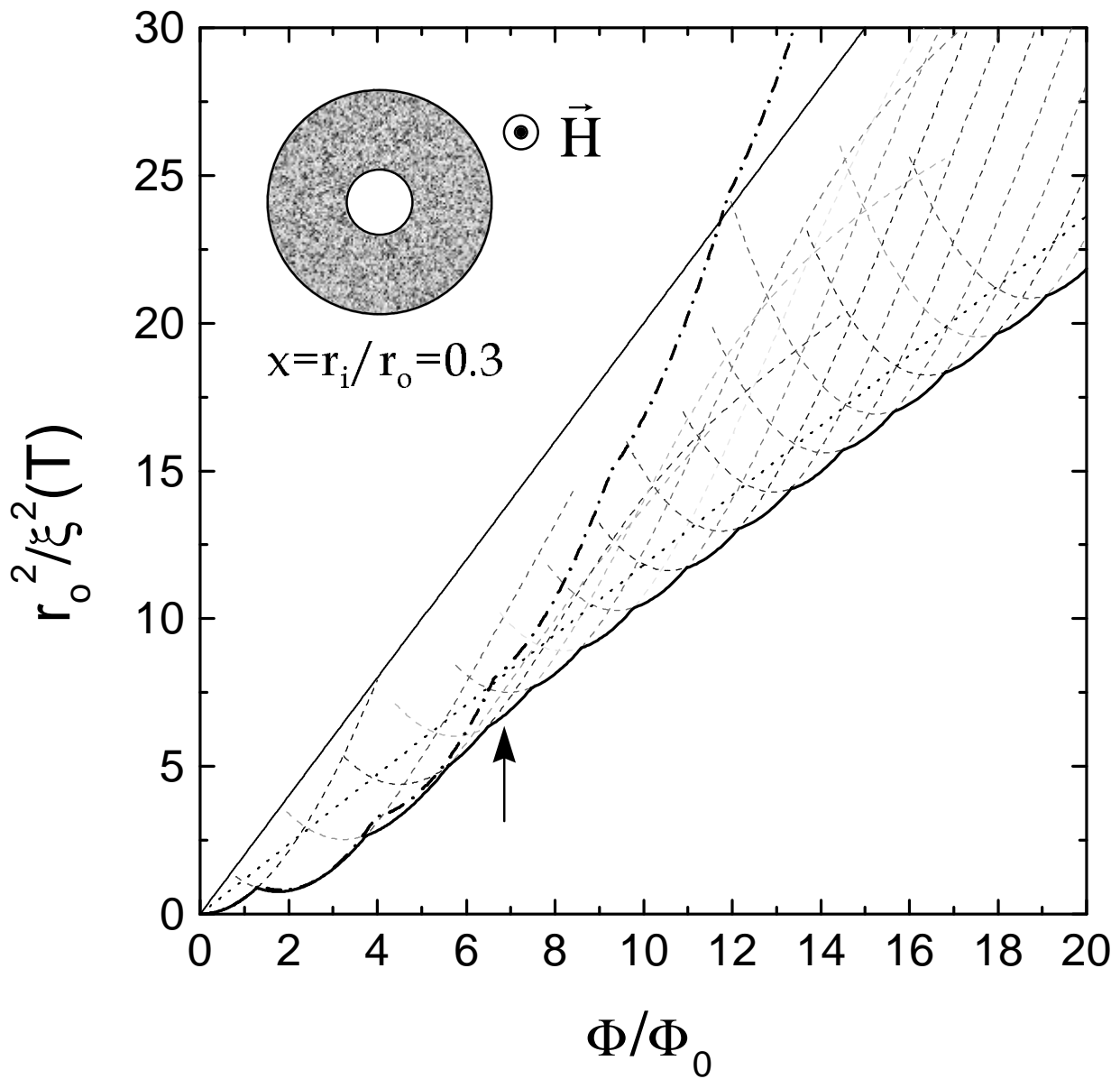


Fig. 1b
Bruyndoncx et al.

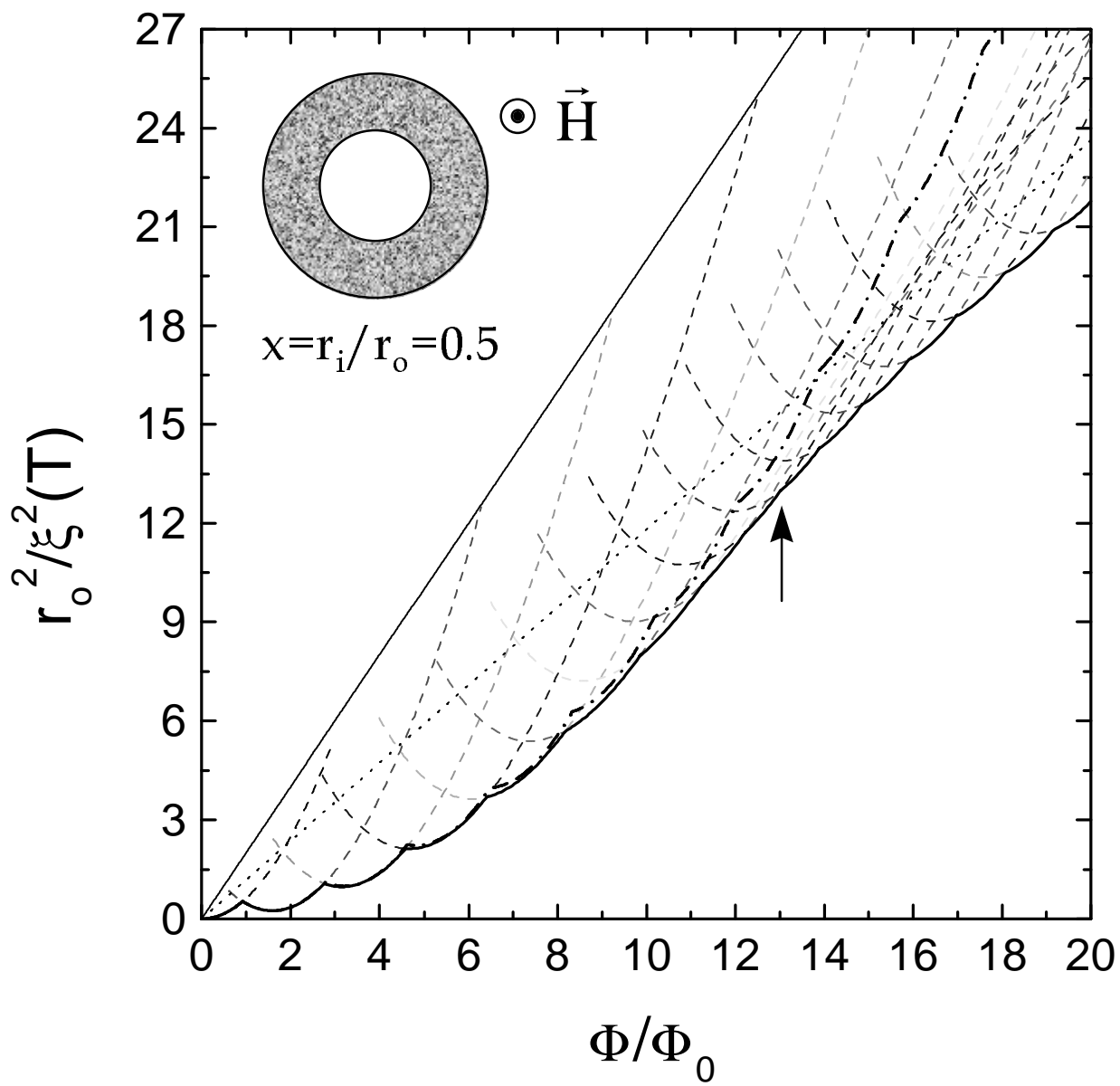


Fig. 1c
Bruyndoncx et al.

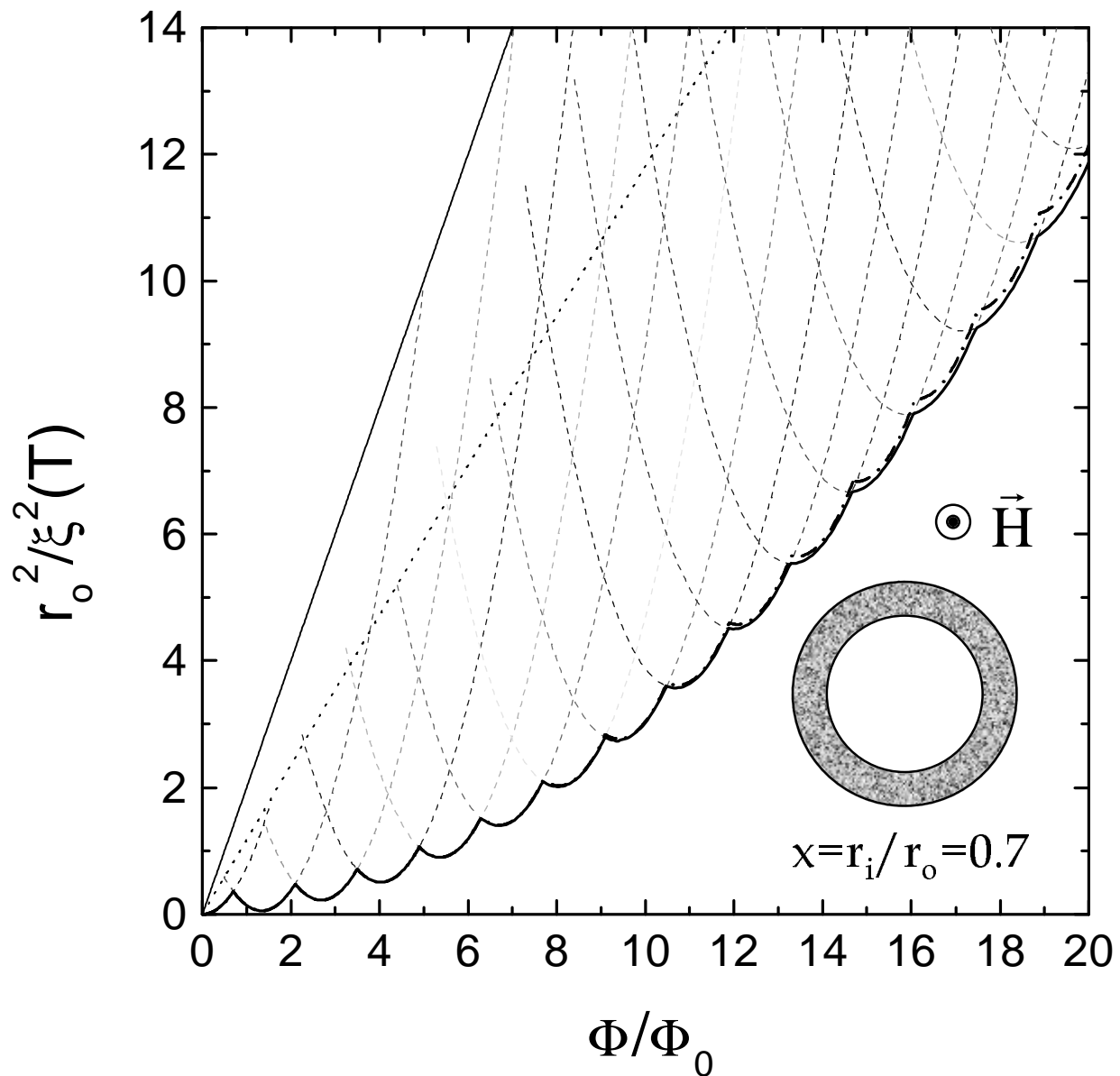


Fig. 1d
Bruyndoncx et al.

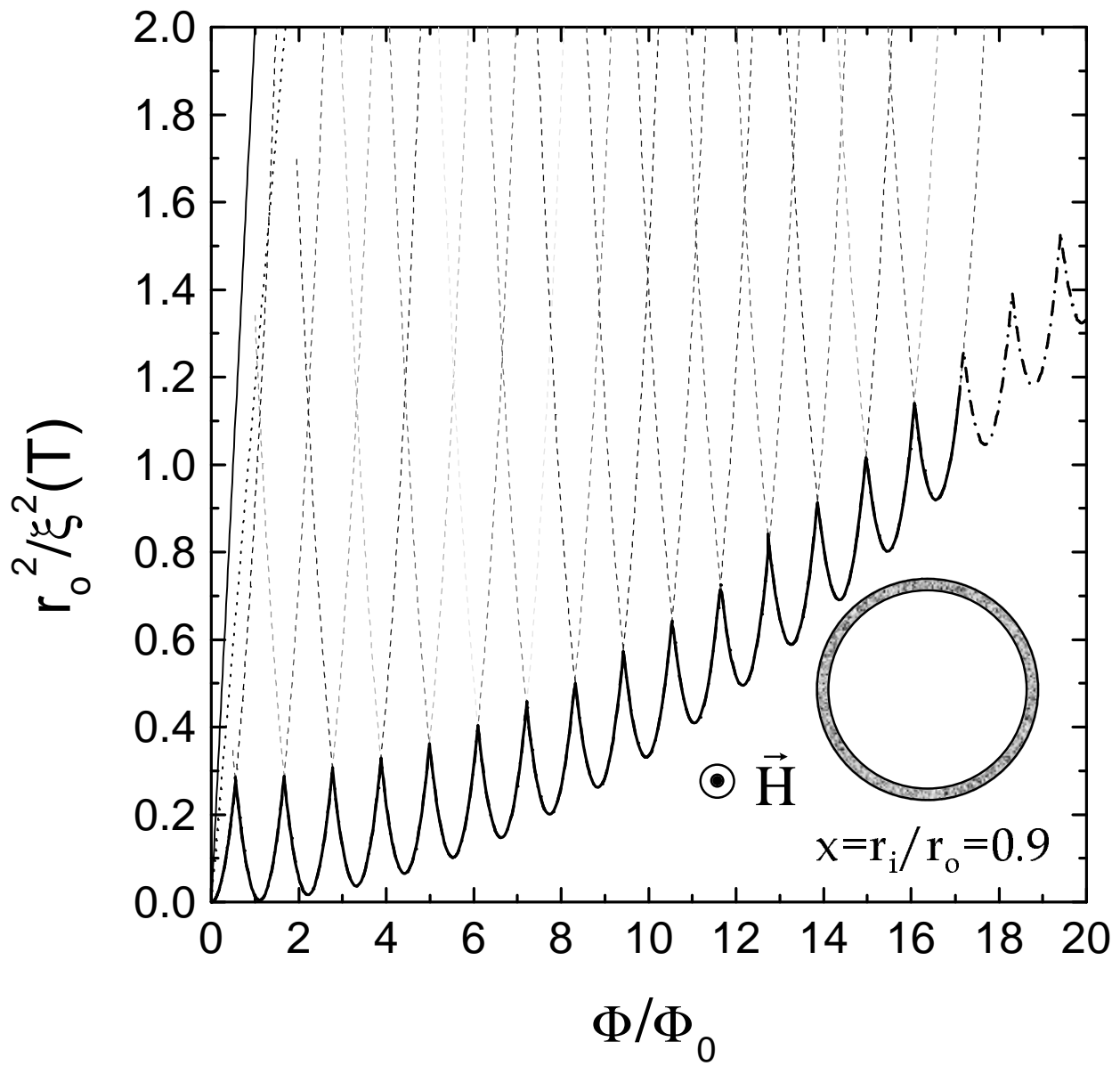


Fig. 1e
Bruyndoncx et al.

This figure "KUMFIG2.JPG" is available in "JPG" format from:

<http://arxiv.org/ps/cond-mat/9907341v1>

This figure "KUMFIG3.JPG" is available in "JPG" format from:

<http://arxiv.org/ps/cond-mat/9907341v1>

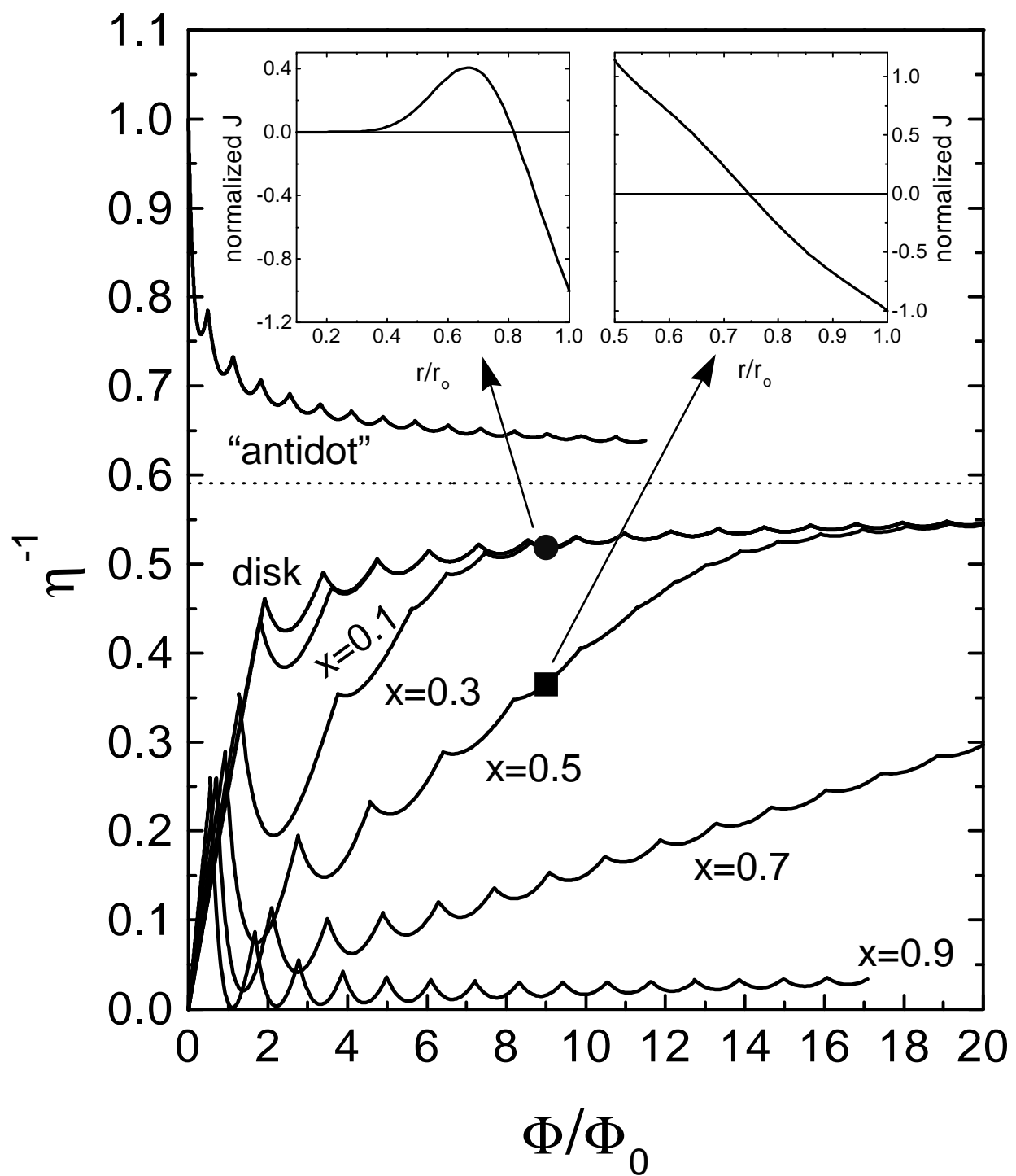


Fig. 4
Bruyndoncx et al.

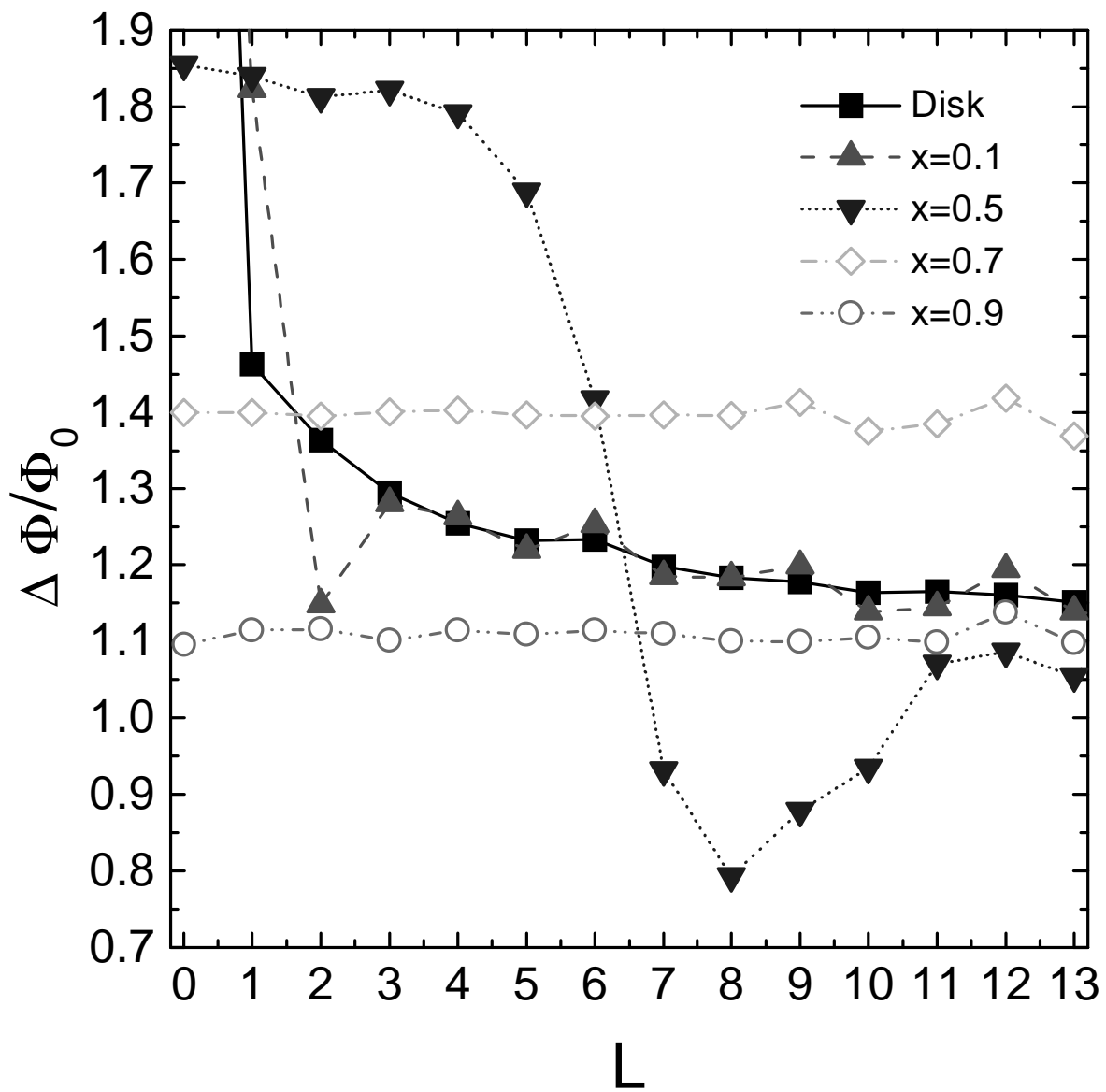


Fig. 5
Bruyndoncx et al.